Chitosan/collagen-based hydrogels for sustainable development: Phycocyanin controlled release

Youssra Ben Azaza, Arie van der Lee, Suming Li, Moncef Nasri, Rim Nasri

Chitosan/collagen-based hydrogels for sustainable development: Phycocyanin controlled release

Youssra Ben Azaza [a, *], Arie van der lee [b], Suming Li [b], Moncef Nasri [a], Rim Nasri [a, c]

[a] *Laboratory of Enzyme Engineering and Microbiology, University of Sfax, National Engineering School of Sfax, P.O.B. 1173-3038, Sfax, Tunisia*
[b] *Institut Européen des Membranes, IEM, UMR 5635, Univ Montpellier, ENSCM, CNRS, Montpellier, France*
[c] *Higher Institute of Biotechnology of Monastir, University of Monastir, P.O.B. 5000, Monastir, Tunisia*

ARTICLE INFO

Keywords:
Composite hydrogels
Phycocyanin
Structural property
In vitro release

ABSTRACT

Marine biopolymers obtained from fishery by-products, such as chitosan and collagen, are sustainable alternatives to developing eco-friendly hydrogels. This work focused on the development of composite hydrogels based on blue crab chitosan (Cs) and bluefin tuna collagenous protein (BTCP), at different concentrations (10%, 20%, and 50%; w/w Cs), by using a freezing/thawing approach. Cs-BTCP composite hydrogels were characterized in terms of structural, morphological, thermal, mechanical, rheological, and antioxidant properties. A highly interconnected porous structure is shown for all the freeze-dried composite chitosan hydrogels by SEM imaging. Additionally, by increasing the concentration of BTCP, the porosity, and swelling degree of the composite hydrogels were improved. Data also revealed that BTCP addition enhanced the elasticity and mechanical resistance of composite hydrogels, especially HG prepared with 50% of BTCP, which explain its high swelling ability which reaches 2160% compared to 1396% for HG-C, at pH 5.5. HG-50 was selected for the *in vitro* release study of phycocyanin as a bioactive molecule and the results revealed that the release depends on the medium pH. Kinetic studies show that phycocyanin release is mainly governed by drug diffusion. Therefore, pH-sensitive Cs-BTPC composite hydrogels could provide an appropriate and supportive microenvironment for the loading and administration of drugs.

1. Introduction

Hydrogels constitute a three-dimensional network composed of hydrophilic polymers cross-linked through inter-molecular or intra-molecular forces of attraction (Ahmadi et al., 2015; Darge et al., 2019). They can absorb huge amounts of water up to several thousand times their dry mass (Feng et al., 2014) while maintaining their dimensional stability (Ahmed, 2015; Rasool et al., 2019). Depending on the nature of cross-link junctions, hydrogels can be divided into two categories, chemical hydrogels crosslinked by covalent bonds (Chen et al., 2021; Liu et al., 2019) and physical hydrogels crosslinked by non-covalent interactions (hydrophobic, hydrogen, ionic) which depend on several environmental factors such as temperature, ionic concentration, pH (Duceac et al., 2021; Phan et al., 2022). Hydrogels can be made from a variety of materials that are generally classified as synthetic (acrylic polymers) or biobased polymers (chitosan, collagen, and proteins) (Shi et al., 2016; Zhou et al., 2022).

Hydrogels based on the self-assembly of biomolecules including polysaccharides and proteins have emerged as a promising platform for biomedical applications (Xing et al., 2016), for controlled release of antimicrobial agents to tissue (Song et al., 2020) and for flexible sensing applications (Bai et al., 2021; Wang et al., 2022), benefiting from their excellent properties such as their inherent bio-

* Corresponding author.
E-mail addresses: youssrabenazaza@gmail.com, youssra.benazaza@enis.tn (Y.B. Azaza).

compatibility, biodegradability, stretchability, mechanical conformability and conductivity, biosafety and flexible environmental responsiveness.

Among biomolecules, chitosan has attracted great attention as one of the most promising candidates for the synthesis of hydrogels because of its excellent biocompatibility, biodegradability, and antibacterial activity (Guo et al., 2019; Mohebi and Shahbazi, 2016). Chitosan is a positively charged linear copolymer with a random arrangement of β-(1–4)-linked D-glucosamine and N-acetyl-D-glucosamine, obtained from the deacetylation of chitin. Chitosan is widely exploited in various fields such as food, cosmetics, pharmacy, medical applications and drug administration thanks to its gelling power, low toxicity, and ability to serve as a matrix for the incorporation of bioactive agents. Hydrogel-based controlled release systems have become a major area of research. The release is generally governed by two mechanisms, drug diffusion and/or hydrogel degradation depending on the hydrogel composition and drug solubility (Gull et al., 2020). Recently, there has been growing interest in the formulation of composite or hybrid systems, which makes it possible to adjust and optimize the structure of the materials with improved functionality and performance.

The innovation of this research is the development of the maritime sectors while valuing the marine by-products, called blue economy. The development of high-added-value products, from the transformation of wastes from the food processing industry, has been given priority in recent years due to the detection of a broad range of biopolymers that could find applications in several fields. For this reason, this study aims to valorize the carapaces of the blue crab (*Portunus segnis*) and the bluefin tuna (*Thunnus thynnus*), to extract the famous chitosan and the bluefin tuna collagenous protein. Therefore, this work's objective was to develop and characterize hydrogels based on chitosan, enriched with bluefin tuna collagenous protein. This chitosan-collagen complex has been considered an excellent matrix for the development of promising material for tissue engineering or drug delivery applications (Magli et al., 2020; Pita-López et al., 2021). Different preparation methods have been used according to the final intended application, such as crosslinking by chemical reaction. Unfortunately, these conventional crosslinking methods involve the use of toxic reagents as crosslinkers and lead to the formation of biomaterials that may be harmful to human health and the environment. The present work involves a strategy based on the physical interaction between the functional groups of the biopolymer chains through non-covalent interactions to obtain a final biomaterial with both polysaccharide and protein properties. The physicochemical properties of hydrogels were assessed by fourier transform infrared spectrometry (FT-IR), X-ray diffraction (XRD) and scanning electron microscopy (SEM). In addition, thermal, mechanical, swelling, biodegradability, rheological and antioxidant properties were also evaluated. Phycocyanin was loaded into the network of hydrogels as a model drug for the evaluation of *in vitro* drug administration at different pH values.

2. Materials and methods

2.1. Materials

The bluefin tuna (*Thunnus thynnus)* by-products and blue crab *(Portunus segnis*) were obtained, under fresh conditions, from a fishery market located at Sfax City, Tunisia. Bluefin tuna by-products were subjected to a series of washing, cutting, grinding, and storage steps at −20°C in polyethylene bags for later use.

Phycocyanin from *Spirulina* sp. was purchased from Sigma Aldrich. 2, 2-diphenyl-1-picrylhydrazyl (DPPH), ferrozine (3-(2-pyridyl)-5,6-diphenyl-1,2,4-triazine), potassium ferricyanide, trichloroacetic acid (TCA), $FeCl_3$, $FeCl_2$, ethylenediaminetetraacetic acid (EDTA), NaOH, ethanol, hexane, hydrochloric acid (HCl) and acetic acid were purchased from Sigma Chemical Co. (St. Louis, MO, USA). All chemicals and solvents were of analytical grade and used as received.

2.2. Preparation of bluefin tuna collagenous proteins

Collagenous proteins were extracted from blue tuna by-products as follows. First of all, tuna by-products were crushed and homogenized with distilled water at a ratio of 1:10 (w/v). Afterward, the pH of the homogenate was adjusted to 5.0 with 1 M HCl solution and the solution was gently stirred for 18 h at 50 ˚C to solubilize the collagenous proteins. After centrifugation at 8000*g* for 30 min, the pH of soluble proteins recovered in the supernatant was adjusted to 7.0 with 2 M NaOH solution. Finally, the powdered bluefin tuna collagenous proteins (BTCP) were spray-dried using a Mini Spray Dryer B-290 apparatus (BÜCHI Labortechnik AG, Flawil, Switzerland). The inlet air temperature was set at 170 ˚C and the outlet air temperature was 80 ˚C.

The moisture was identified according to the AOAC standard method (AOAC Official Method, 2019). The total protein content (N% x 6.25) of the protein isolate was determined by using the Kjeldahl method. The yield of BTCP recovery was calculated based on the wet weight of raw materials.

2.3. Preparation of blue crab chitosan

Chitosan obtained from *Portunus segnis* blue crab shells was prepared as described by Hamdi et al. (2019). Blue crab shells were carefully washed with tap water to remove impurities, and heated for 20 min at 90 ˚C. Then, the shells were dried at room temperature and powdered in a Moulinex® blender. For chitin extraction, two main steps were involved: i) demineralization step was performed chemically under stirring in a solution of HCl (0.55 M) at a ratio of 1/10 (m/v), using three repeated acid baths, for a duration of 30 min each bath, and ii) enzymatic deproteinization step was conducted using Purafect® at an enzyme/substrate ratio of 5 U/mg of protein for 3 h under optimal enzyme conditions (pH 10.0, 50 ˚C). Finally, the conversion of chitin to chitosan involved the deacetylation reaction. The recovered chitin was treated with 12.5 M NaOH at a ratio of 1/10 (w/v) for 4 h at 140 ˚C, to obtain perfectly water-soluble chitosan in acidic conditions. After filtration, the residue was washed with distilled water until the pH was neutral, and the crude chitosan (Cs) was dried at 50 ˚C overnight.

The degree of deacetylation (DD) of Cs, evaluated by potentiometric titration, was shown to be significantly high (90.39 ± 1.36%) as reported by Hamdi et al. (2018). Moreover, the average molecular weight of the obtained Cs was estimated to be 115,000 g mol-1 based on size exclusion chromatography (SEC) analysis.

2.4. Development of composite hydrogels

Hydrogels (HGs) were prepared based on the freezing/thawing approach as reported by Duan et al. (2015). Firstly, 3 wt% Cs dissolved in an alkaline solution (4.5 wt % LiOH, 7.5 wt % KOH and 8.5 wt % urea) was mixed with BTCP at different concentrations (10%, 20% and 50%; w/w Cs). Thereafter, the reaction mixtures were maintained at −30 °C for 12 h until complete freezing, followed by a thawing step at 20 °C for 4 h under intensive stirring until a clear and transparent solutions were formed. The freezing/thawing process was repeated twice and the resulting solutions were kept at 60 °C for 1 h (solvent evaporation technique), promoting the formation of physical gels. After exhaustive washing with ultra-pure water, the formed HGs were immersed in absolute ethanol solution for 3 days at 4 °C to improve gel maturation. Composite hydrogels obtained with 10%, 20% and 50% BTCP were named, respectively, HG-10%, HG-20% and HG-50%. Chitosan hydrogel based only with chitosan (HG-C) was also prepared as a control according to the same process.

2.5. Characterization of composite hydrogels

2.5.1. Moisture content and water holding capacity

The moisture content (MC) of HGs was determined according to the AOAC method (AOAC Official Method, 2019). The MC was determined by drying about 100 mg of each sample at 105 °C for 24 h until the dry weight of the sample was reached (constant weight). The MC of the HGs was determined by measuring the mass loss and expressed as follows:

$$MC\ (\%) = \frac{[W_0 - W]}{W_0}\ x\ 100 \tag{1}$$

where W_0 and W are the respective masses (g) of composite hydrogels before and after drying at 105 °C. The experiment was carried out in triplicate and the results are mean values.

The water-holding capacity (WHC) of HGs was carried out as reported by Rawdkuen et al. (2009). Briefly, after cutting the HGs into small cylindrical pieces, they were weighed. Then, samples were placed between 1 piece of filter paper on top and 2 pieces of filter paper below. A standard weight (2 kg) was placed on the top of the sample for 2 min, and then the sample was removed from the papers and weighed again. The WHC of the HGs is expressed in %.

2.5.2. Scanning electron microscopy

The structure of HGs was determined by scanning electron microscopy (SEM, Hitachi S4800) at an acceleration voltage of 2.0 kV. The hydrogel sample was quenched into liquid nitrogen. The frozen sample was cut into small square pieces and then sprayed with gold before observation.

2.5.3. FT-IR Spectroscopy

FT-IR analysis was performed using a spectrometer (Agilent Technologies, Carry 630 series) equipped with an attenuated reflection accessory (ATR) containing a diamond crystal/ZnSe. An average of 32 scans was collected with 4 cm^{-1} resolutions in the wavenumber range of 650–4000 cm^{-1}. Data analysis was performed using OMNIC Spectra software (ThermoFisher Scientific software).

2.5.4. X-ray diffraction (XRD)

XRD analysis of the prepared HGs was carried out on a Philips diffractometer using a Cu Kα radiation source (k = 1.5406 °A). The samples were scanned continuously at a voltage of 40 kV and a current of 30 mA in the ranging 2θ from 7 to 40°.

2.5.5. Thermogravimetric analysis (TGA)

TGA thermograms were recorded on high-resolution TGAQ 500 analyzers (TA Instruments). Measurements were made in the temperature range from 25 to 700 °C at a heating rate of 20 °C/min.

2.5.6. Mechanical testing

Compression tests were performed using the universal test Dynamique Mechanical Analyser "DMA50" (Metravib, Brand of ACOEM, France) at 25 °C and a speed of 1 mm/min. The stress-strain curves for hydrogel compression-recovery were obtained by compressing the samples to 1%, 2%, 3%, 4%, 5%, 6% and 7%, and then returning at the same speed (1 mm/min). The hysteresis of the stress-strain curve was recorded.

2.5.7. Rheology measurements

The storage modulus (G′) and loss modulus (G″) of prepared HGs were determined using a rheometer apparatus (Physica MCR. Anton Paar. GmbH. France) equipped with 25 mm parallel plates. Liquid paraffin was used to minimize water evaporation from hydrogels. The HG sample is a 25 mm diameter disc with a thickness of about 2 mm. The linear viscoelastic response region was judged via a frequency (ω) from 0.01 to 6.2 rad/s with a constant strain sweep of γ = 0.01% at T = 25 °C. Dynamic experiments were performed with a frequency range of 0.1–100 rad/s at a strain amplitude of γ = 0.1%.

2.5.8. Antioxidant potentials of composite hydrogels

2.5.8.1. DPPH free radical-scavenging assay. The DPPH free radical-scavenging activity of HGs was assessed by using a literature method of Bersuder et al. (1998), with slight modifications. The samples (30 mg) were allowed to react with DPPH (0.02%) radicals in an ethanol solution. DPPH, which has a dark purple color in its radical form, becomes colorless after a reaction with an anti-radical antioxidant. A significant free radical scavenging activity of DPPH corresponds to a low absorbance at 517 nm. The DPPH radical-scavenging activity (%) was carried out in duplicate and calculated using the following equation:

$$DPPH\ (\%) = \frac{[A_c + A_b - A_S]}{A_c}\ x\ 100 \tag{2}$$

where A_c, A_b, and A_s represent the absorbance of the control (containing all reagents except the sample), the blank (containing all reagents except the DPPH solution), and the composite films with the DPPH solution, respectively.

2.5.8.2. Ferrous ion-chelating activity. It is a colorimetric method based on the monitoring of the formation of a red chromophore complex (Fe^{2+}-ferrozine). The maximum absorbance of this complex is located at a wavelength of 562 nm. The chelating antioxidant activity of HGs toward ferrous ions (Fe^{2+}) was measured according to the method reported by Decker and Welch (1990), with some modifications. Briefly, HG samples (0.5 g) were mixed with 450 μL of distilled water. Then, 50 μl of 2 mM $FeCl_2$, $4H_2O$ and 200 μl of 5 mM Ferrozine (3- (2-pyridyl) −5,6-bis (4-phenyl-sulfonic acid) −1,2,4-triazine) were added, and the reaction mixture was vigorously stirred. After incubation, the absorbance of the solutions was measured at 562 nm. The inhibition percentage of ferrozine-Fe^{2+} complex formation was calculated according to the equation below:

$$Metal\ chelating\ activity\ (\%) = \frac{[A_c + A_b - A_S]}{A_c}\ x\ 100 \tag{3}$$

where A_c, A_b, and A_s represent the absorbance of the control, the blank and the samples, respectively. The test was carried out in triplicate and the results are mean values.

2.5.8.3. Reducing power assay. The ability to reduce iron (III) was performed using the method of Yildirim et al. (2001). Thus, HG sample (30 mg) was added to 1.25 mL of 0.2 M PBS (pH 6.6) and 1.25 mL of 1% (w/v) potassium ferricyanide solution $K_3Fe(CN)_6$. After incubation for 3 h at 50 °C, the reaction was stopped with the addition of 1.25 mL TCA 10% (m/v). Then, the mixture was centrifuged for 10 min at 3500 g. The supernatant (1.25 mL) was mixed with 1.25 mL distilled water and 0.25 mL 1% (m/v) ferric chloride. After incubation at room temperature for 10 min, the absorbance of the resulting solutions was measured at 700 nm. The reducing ability was monitored by measuring the increase in the absorbance at 700 nm. The test was performed in duplicate. BHA was used as a positive control.

2.5.9. Swelling measurements

The swelling degree (SD) of HGs was investigated in distilled water. The pre-weighed dry samples were immersed in excessive distilled water and kept for 24 h at room temperature until equilibrium swelling was reached. The swollen HG was removed carefully, ripped with filter papers, and then weighed again. The SD was calculated as follows:

$$SD\ (\%) = \frac{[w_s - w_d]}{w_d}\ x\ 100 \tag{4}$$

where w_s is the mass of the swollen HG and W_d is the mass of dried HG before swelling at time t.

2.5.10. In vitro degradation study

The *in vitro* degradation study of HGs was established as described by Yan et al. (2019). Briefly, the raw cylindrical samples (100 mg) were immersed into 10 ml phosphate buffered saline (PBS) at pH 7.4 (physiological microenvironment simulation) and 5.5 (acidic microenvironment), at 37 °C and under gentle shaking (~ 100 rpm). Then, samples were removed from the medium and weighed at pretime points time-points. The degree of *in vitro* degradation was expressed by the remaining weight of HGs, after oven-drying during 48 h at 60 °C and calculated as follows:

$$Remaining\ weight\ ratio\ (\%) = \frac{w_t}{w_i}\ x\ 100 \tag{5}$$

W_t is the remaining hydrogels dry weight after degradation at each selected time interval and W_i is the initial hydrogels dry weight.

2.6. Loading capacity and In vitro release studies

Phycocyanin (Ph) was chosen as a model of bioactive molecules for *in vitro* release experiments. Ph was incorporated in the hydrogel's matrix by soaking wet HG (30 mg) in 10 mL of Ph aqueous solution (3 mg/L) for 48 h. The quantitative amount of loading capacity (%LC) of Ph in HG was determined according to the below formula:

$$LC\ (\%) = \frac{W_L}{W_{HG}}\ x\ 100 \tag{6}$$

where W_L is the weight of the loaded Ph in the HG and W_{HG} is the weight of the HG, respectively.

The release behavior of the loaded Ph from HGs was evaluated in PBS at different pH values (pH 5.5 and 7.4). Ph-loaded HG samples (30 mg) were suspended in 10 mL PBS buffer at 37°C and at 50 rpm in a shaking incubator. An aliquot of the supernatant (1 mL) was periodically withdrawn at different intervals from 1 to 48 h and replaced by 1 mL fresh medium. The amount of released Ph was obtained considering the cumulative quantity of Ph in each of the release system, based on a previously established calibration curve (Agilent Technologies UV–visible spectrometer, Carry 630 series) at 620 nm. All measurements were performed in triplicate.

2.7. Release kinetic studies

To well describe the release behavior, the kinetics of Ph release was studied by applying four different kinetic models, namely zero order (cumulative percent drug release vs time), first order (log cumulative percent drug release vs time), Higuchi's kinetics (cumulative percent drug release vs time), and Korsmeyer-Peppas equation (log cumulative percentage of drug release vs log time). The different kinetic models were given in the following equations:

$$Zero\ order\ model: \quad \frac{Qt}{Q\infty} = Kt, \tag{7}$$

$$First\ order\ model: \quad \frac{Qt}{Q\infty} = 1 - e^{-Kt}, \tag{8}$$

$$Higuchi\ model: \quad \frac{Qt}{Q\infty} = Kt^{1/2t}, \tag{9}$$

$$Korsmeyer - Peppas\ model: \quad \frac{Qt}{Q\infty} = Kt^{n}; \tag{10}$$

where Qt represents the percentage of Ph released at time t, and Q∞ represents the total percentage of Ph released; Qt/Q∞ is the fractional release of drug at time t. k is the release rate constant and n is the diffusional exponent which could indicate the Ph release mechanism and t is the time.

2.8. Statistical analysis

Data were expressed as mean ± SD and statistically analyzed using the one-way analysis of variance ANOVA procedure with SPSS ver. 20.0 professional edition (SPSS, Inc., Chicago, IL, USA). When $p < 0.05$, differences were considered as statistically significant.

3. Results and discussion

3.1. Characterization of Cs and Cs-BTCP hydrogels

3.1.1. Moisture content and water holding capacity

The MC and the WHC of HGs were determined and the results are shown in Table 1. The results revealed that all HGs present high moisture content values, ranging from 88.11% to 96.70% ($p < 0.05$). MC is one of the important properties, which distinguish HGs from other biomaterials. Hydrogels are described by their ability to absorb and retain a large amount of water in their swollen state like soft tissues. Therefore, they could be a promising material in biomedical application (Chai et al., 2017). In fact, the water-rich structure facilitates the transport of molecules, water and oxygen between the external environment and the gel, mimicking, therefore, cell function in the body (Dimatteo et al., 2018). The capacity of the composite HGs to hold water was also studied. As shown in Table 1, the incorporation of BTCP to the chitosan matrix significantly improved the WHC values of composite HGs, which increased from 29.02% for HG-C to 36.62%, 60.62% and 66.95% for HG-10%, HG-20% and HG-50%, respectively. Therefore, the addition of BTCP improves the MC and the WHC of HG-C matrix which could be explained by the hydrophilic nature of BTCP.

3.1.2. Morphology

The internal microstructure of the cross-section HGs was determined by the SEM. As depicted in Fig. 1, all freeze-dried HGs present an interconnected pore network. The pores are formed by the removal of ice water during freeze-drying (Guo et al., 2019). Nevertheless, differences are observed between HG-C and BTCP containing HGs. HG-C presents a uniform lamellar structure (Arulmoorthy et al., 2020). Additionally, we noted hydrogel shape of the hydrogel's pores shifted from fibril to a spherical structure

Table 1
Physicochemical characterization, in terms of moisture content (MC, %) and water holding capacity (WHC, %) of Cs-BTCP composite hydrogels.

	HG-C	HG-10%	HG-20%	HG-50%
MC (%)	88.11 ± 0.84 [a]	92.57 ± 0.48[b]	94.42 ± 0.19[c]	96.70 ± 0.64[d]
WHC (%)	29.02 ± 0.10[a]	36.62 ± 0.52[b]	60.28 ± 0.99[c]	66.95 ± 0.33[d]

MC: moisture content; **WHC**: water holding capacity. [a-d] Different letters in the same line indicate a significant difference ($p < 0.05$).

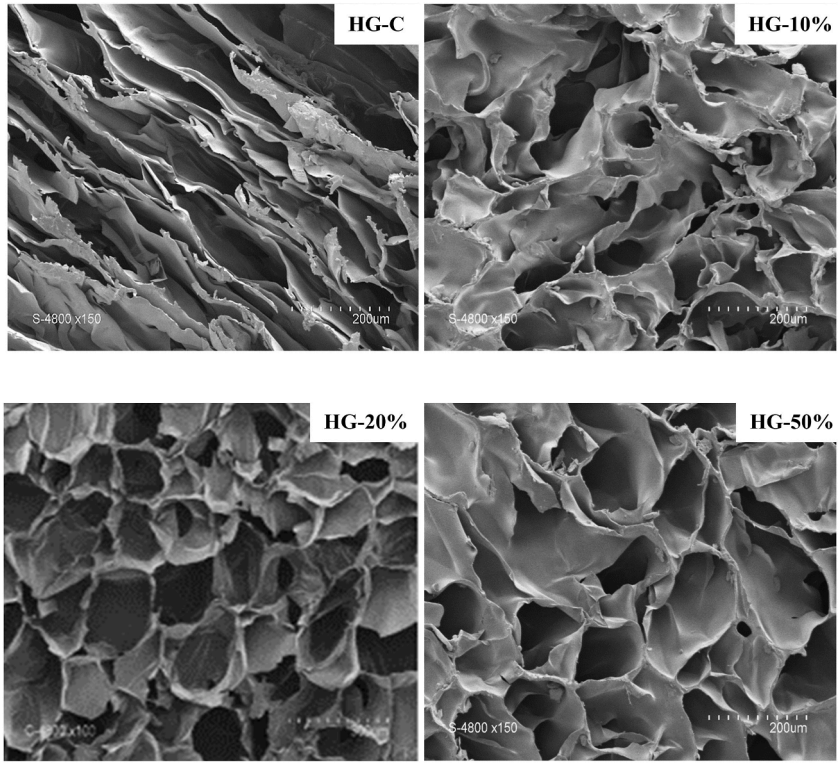

Fig. 1. SEM images cross sections.

with homogeneous pores distribution. In fact, the SEM images showed a better pore structure as the BTCP concentration increased. As expected, when BTCP was added to the Cs matrix, the HGs pore size was reduced remarkably, indicating an enhanced cross-linking density of hydrogels and forming a robust network structure with covalent linkage and intermolecular entanglements (Chang et al., 2008). As reported by Feki et al. (2020) and Hamdi et al. (2020), the addition of *Falkenbergia rufolanosa* polysaccharide and blue crab protein isolate into the chitosan matrix led to the decrease of HGs pore size.

Overall, the porous Cs-BTCP composite HGs could be a promising candidate for the development of controlled release systems due to their porosity and ability to entrap bioactive drugs and proteins (Lima et al., 2018).

3.1.3. Fourier transformed infrared (FT-IR) analysis

FT-IR spectra of HG-C and Cs-BTCP composite HGs are illustrated in Fig. 2A. FTIR HG-C spectrum presents a broad peak in the range of 3400-3200 cm^{-1} attributed to an amine -OH symmetrical vibration. The band appearing at 2900 cm^{-1} corresponds to the C–H asymmetric and symmetric stretching. Additionally, specific bands for chitosan are detected, -C = O (1644 cm^{-1}), -CH (1415 cm^{-1}), and glycosidic rings of chitosan (1079-1025 cm^{-1}) (Hamdi et al., 2020).

Composite hydrogels spectra showed distinguishing peaks of proteins at 1644 cm^{-1} (Amide I) associated with a carbonyl elongation vibration (-C = O), 1584 cm^{-1} (Amide II) assigned to the elongation vibration of the -NH bond and an extensional vibration of the -CN bond and 1446 cm^{-1} (Amide III) assigned to a combination of previous vibrations with deformation vibrations of $-CH_2$ groups. Compared to the HG-C spectrum, an increase in the intensity of Amide A was noted (Fig. 2A), indicating the formation of intermolecular hydrogen bonds between BTCP and Cs (Voron'ko et al., 2016). In addition, an increase in the intensity of the amide I peak (1644 cm^{-1}) was observed. Moreover, there is a shift in the frequency of amide III to a higher wavenumber for all composite films (from 1415 cm^{-1} to 1446 cm^{-1}). These outcomes indicate the presence of changes in the conformation of polypeptide chains of BTCP (Bealer et al., 2020; Hosseini et al., 2015).

3.1.4. X-ray diffraction (XRD)

To further investigate the structural changes in the matrix of the HG-C as well as Cs-BTCP composite HGs during dissolution in the aqueous alkaline/urea system and gelation, XRD analysis was performed. The XRD profiles of the HGs were studied between 5 and 40° of 2θ (Fig. 2B). The XRD pattern of HG-C showed crystalline a peak at around $2\theta = 12°$, $2\theta = 20°$, $2\theta = 30°$ and $2\theta = 31°$. Moreover, with increase of BTCP content, the diffraction peaks showed weakened intensity and some peaks almost disappeared. These results suggested that there were good compatibility and interaction between Cs and BTCP molecules in the hydrogel matrix, as the addition of BTCP in HG-C reduces the crystallinity of HG-C due to hydrogen bonding between Cs and BTCP.

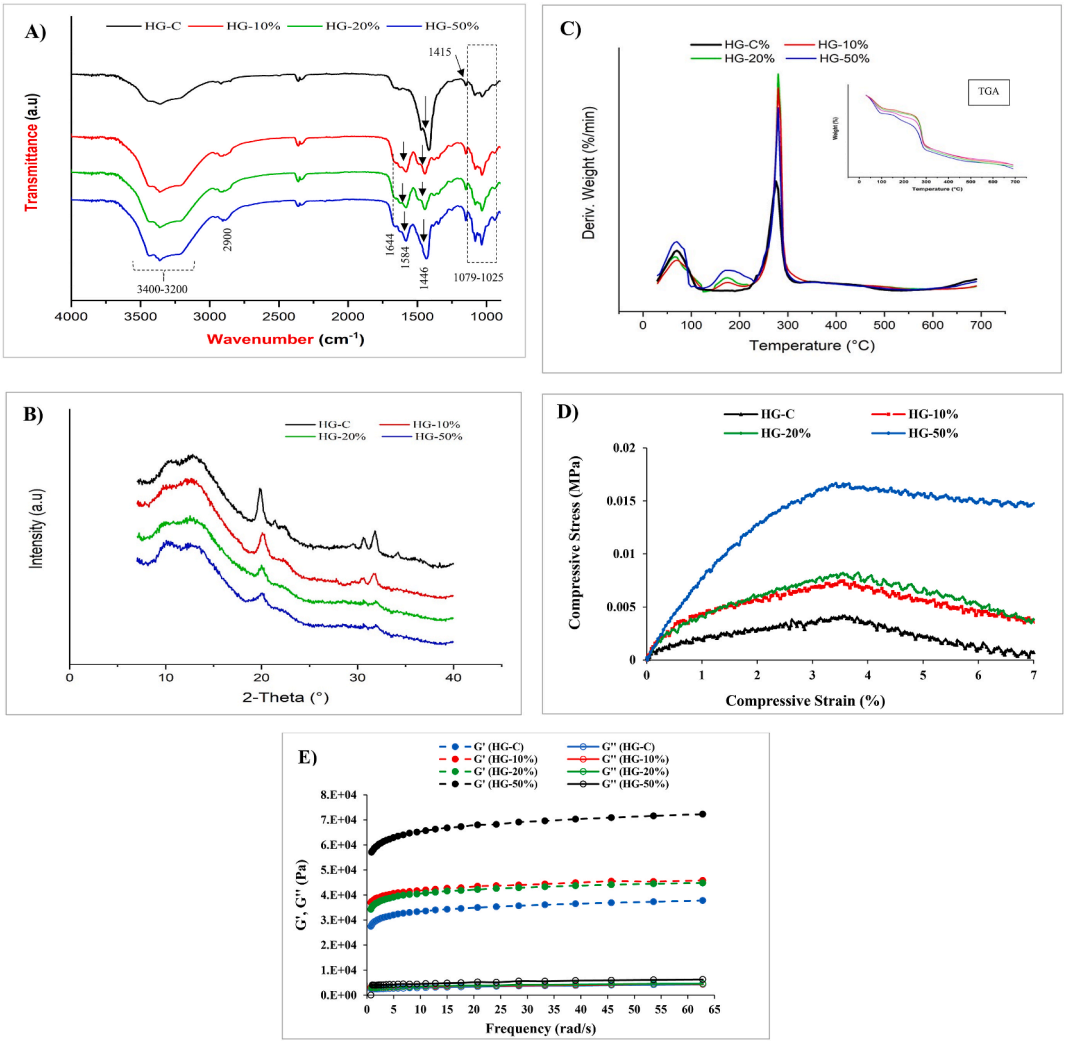

Fig. 2. ATR-FTIR profiles (**A**), XRD patterns (**B**), DTG and ATG thermograms (**C**), Mechanical behavior: Compressive stress vs compressive strain profiles (**D**), Rheological behavior at $\gamma = 0.01\%$ and $T = 25$ °C (**E**) of Cs hydrogel and Cs-BTCP composite hydrogels.

3.1.5. Thermal properties

Thermal profiles of HGs were studied through ATG analysis. The DTG thermogram of HG-C, shown in Fig. 2C, presents two main weight loss stages. The first weight loss, which occurred at temperatures ranging between 50 and 100 °C, corresponded to the removal of moisture (dehydration), while the second one, recorded at Tmax (temperature at which sample lost maximum of its weight) of about 275 °C, was attributed to the decomposition of chitosan. Regarding TGA curves of composite HGs, three phases of weight loss were noted (Fig. 2C): i) The first one corresponded to the removal of moisture; ii) The second weight loss detected at Tmax about 174 °C, may be related to the degradation of BTCP; and iii) The third peak of weight loss recorded at Tmax about 280 °C was attributed to the decomposition of the chitosan matrix. The obtained results indicate that the incorporation of BTCP led to the creation of a polymeric network (Cs-BTCP) slightly more resistant to thermal degradation than those based on pure Cs. Similar results were observed by Hamdi et al. (2020) who reported that the thermal stability of chitosan hydrogel was positively correlated with the amount of added blue crab protein isolate.

3.1.6. Mechanical analysis

To assess the mechanical strength, compressive stress-strain curves of achieved HGs are illustrated in Fig. 2D. At low deformation values ($< 3.5\%$), an elastic deformation behavior, shown in the diagram by a line, was observed. Up to 3.5% compression strain, the stress augmented sluggishly, subsequently a plastic deformation, due to the bonds breaking or structure rearrangement (Chen et al., 2019). The study of the mechanical behavior of HGs in a compression regime show that HG-C was relatively brittle and non-elastic as it had a low compressive strength of 0.004 MPa with a minimal strain (3.5%) prior to rupture (Jafari et al., 2019). This low mechanical strength of HG-C could be explained by its high crystallinity, which is reported above in the XRD results, resulting in a more fragile and less elastic HG-C.

A positive correlation between the BTCP concentration and the mechanical strength of composite HGs was observed in Fig. 2D. In fact, the compressive stress of rupture for HG-50% increased dramatically reaching 0.018 MPa, but the elasticity did not change as they both broke at a strain of 3.5% ($p < 0.05$). So, the HG-50% was the most resistant to deformation followed by HG-20% et HG-10%. Consequently, the synergistic effect of Cs and BTCP contributes to the structural resistance of the hydrogel network and the formation of tighter HGs networks with better mechanical properties.

3.1.7. Viscoelasticity analysis

The rheological properties of composite HGs, storage modulus (G′) and loss modulus (G″), as a function of frequency (ω) from 0 to 62.8 rad/s with a constant strain sweep of $\gamma = 0.01\%$ at $T = 25$ °C, were evaluated (Fig. 2E). Generally, the G′ represents elastic property while the G″ refers to viscosity. For all prepared HGs, the G′ values were independent of frequency and remain greater than G″ values (G′ > G"), indicating that the HGs manifested higher elastic gel-like behavior. The obtained data reveal the successful formation of strong cross-linked network between polymer chains. Additionally, it is found that the reinforcement of chitosan HGs by BTCP significantly improved hydrogels elasticity ($p < 0.05$). Indeed, the G' values increased from 37 kPa for HG-C to 73 kPa for HG-50% at 62.8 rad/s. This finding could be explained by the fact that the addition of BTCP could increase the hydrogen bonding and enhance the entanglement of polymer chains, leading to a more stable polymeric network structure and much higher G′ value (Wei et al., 2019). Thus, increasing the concentration of BTPC remarkably enhances the stability, strength, and viscoelasticity of the hydrogel network structure (Duan et al., 2015; Marapureddy and Thareja, 2020).

3.1.8. Antioxidant potentials

Data in Table 2 show that the antioxidant potential of composite HGs is clearly higher than HG-C ($p < 0.05$). The various synthesized hydrogels were able to stabilize the free radical's DPPH and reduce the ferric ions (Fe^{3+}), also endowed with an interesting ability to chelate ferric ions. With the increase of added BTCP content, the antioxidant potential is enhanced.

Therefore, the incorporation of BTPC into the Cs-based hydrogel matrix network improved the antioxidant activity of the resulting hydrogels. This can be explained, as mentioned earlier in FT-IR analysis, by improving the availability of free amino groups in composite hydrogels.

3.1.9. Swelling measurements

One of the most interesting properties of hydrogels is their ability to swell and shrink, depending on their surroundings. The pH of the solution can significantly influence the rate of swelling degree of HGs (Raj Singh et al., 2009), by affecting the functional group ionization of molecules on the surface of the hydrogel (Cruz et al., 2019; Wu et al., 2018). To study the effect of pH on swelling rate, HGs were allowed to swell to equilibrium in PBS at pH 5.5 and 7.4. Fig. 3 shown that the SR of hydrogels increased with the increase of the amount of BTCP in HG matrix. The obtained results are in line with those MC and WHC analysis. In fact, the addition of BTCP could improve the hydrophilic nature of composite HGs, promoting their interactions with water molecules. Accordingly, the swelling ability of hydrogels could be attributed directly to its enhanced water content and the largest pores formed (Wei et al., 2017). In addition to the porosity of hydrogels, polarity was also correlated with the ability of hydrogels to absorb water (Hamdi et al., 2020).

On the other hand, HGs showed a pH-dependent swelling behavior (Fig. 3). HG-C showed maximum swelling (1396%) at pH 5.5 vs lower swelling (834%) at pH 7.4, whereas HG-50% showed a sharp increase in swelling among all the different composite HGs with a value of 2160% at pH 5.5 vs a value of 1198% at pH 7.4 ($p < 0.05$). This finding could be attributed to the protonation of amine groups of chitosan at pH 5.5, causing electrostatic repulsion between chains and expansion of the gel network (Islam and Yasin, 2012; Rasool et al., 2019; Wei et al., 2017).

3.1.10. In vitro degradation

In vitro degradation behavior was based on the ability of hydrogels to be biologically degradable, considering their weight loss over time. To simulate physiological and acidic microenvironments, respectively, all HG samples were placed in PBS at pH values of 5.5 and 7.4 for 10 days at 37 °C (Fig. 4). In the degradation analysis experiments, the results showed that, independently of the medium pH and the composition of the hydrogel matrix, all hydrogels gradually degradable over time. As suggested by Tuan Mohamood et al. (2018), the ions in PBS can break the intra and intermolecular hydrogen bonds of polysaccharides, leading to the degradation of polysaccharides-based system.

The results demonstrated also that composite HGs were more stable against degradation than HG-C, regardless of medium pH. It seems that the presence of BTCP in the chitosan matrix was an advantage for the hydrogels to increase their stability against degradation. This finding may be due to the effect of BTCP on the improvement of the cross-linking between both polymers and, therefore, on the strengthening and the density of the composite network structure. These results are consistent with the mechanical strength, the pore size, and the swelling behavior data of the composite HGs. The same results were reported by Feki et al. (2020), who found that

Table 2
In vitro antioxidant activities of Cs-BTCP composite hydrogels.

	HG-C	HG-10%	HG-20%	HG-50%
Radical scavenging activity (%)	97.66 ± 0.95[a]	94.59 ± 0.08[b]	99.28 ± 0.07[b]	100.00 ± 0.16[a]
Reducing power assay	0.136 ± 0.06[a]	0.182 ± 0.01[b]	0.224 ± 0.09[c]	0.33 ± 0.06[d]
Iron chelating effect (%)	86.03 ± 0.41[a]	97.59 ± 0.09[b]	98.45 ± 0.00[c]	100 ± 0.00[d]

[a-d] Different letters in the same line indicate a significant difference ($p < 0.05$).

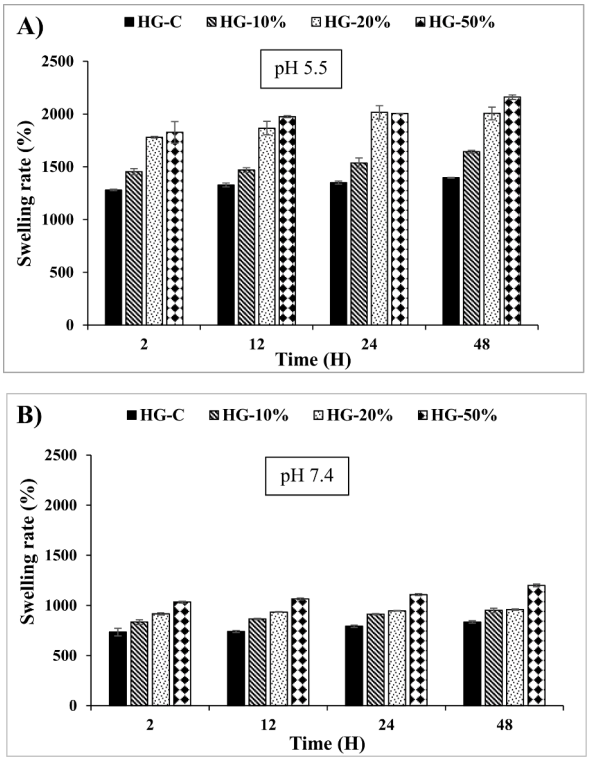

Fig. 3. Swelling behavior of Cs hydrogel and Cs-BTCP composite hydrogels: Swelling rate in PBS buffer solution at pH 5.5 (A); Swelling rate in PBS buffer solution at pH 7.4 (B).

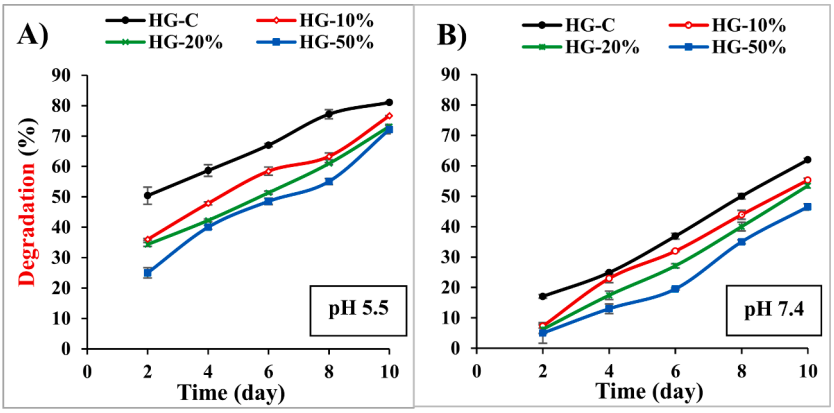

Fig. 4. *In vitro* biodegradation of Cs hydrogel and Cs-BTCP composite hydrogels, in PBS buffer solution at **(A)** pH 5.5 (acidic microenvironment) and **(B)** pH 7.4 (physiological microenvironment simulation), at 37 °C.

the addition of *Falkenbergia rufolanosa* polysaccharide into the chitosan hydrogel matrix improved the stability of the composite hydrogels against the biodegradation process.

Furthermore, hydrogels, in PBS of pH 5.5, undergoes the fastest degradation, compared to samples immersed in PBS of pH 7.4. For example, the degradation rate of composite HGs (HG-10%, HG-20% and HG-50%) was about 76, 73 and 72% in pH 7.4, and about 55, 53, 46.5% in pH 5.5 (Fig. 4A and 4B). Thus, under acidic conditions (PBS pH 5.5), the degradation system was enhanced by inducing the protonation of Cs amino groups (Nie et al., 2016; Xing et al., 2019). Subsequently, the binding of macromolecular chains becomes brittle, resulting in the destruction and decomposition of hydrogel networks. These results corroborate directly with the morphology of the hydrogels based on the SEM images, showing that differences in degradation behavior could be ascribed to a significant increase in pore size, which increased thereby the swell-ability of the HG after immersion in the PBS.

Overall, all these results suggested that HG-50 endowed good stability in PBS, which could trap and release drugs or other bioactive molecules and could be used in the biomedical field as drug delivery devices (Figueroa-Pizano et al., 2018).

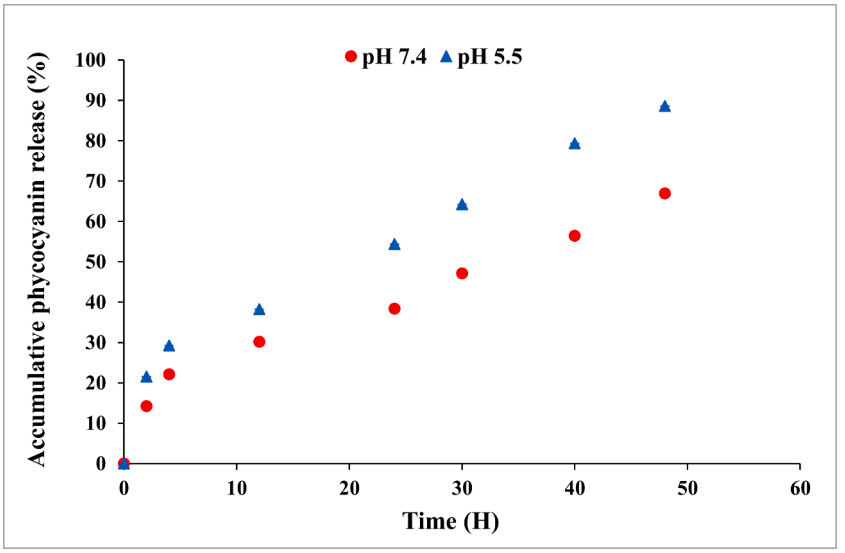

Fig. 5. *In vitro* cumulative release profiles of phycocyanin from HG-50% at pH = 5.5 and pH = 7.4 (37 °C; PBS buffer).

Table 3
Kinetic parameters obtained through fitting to several mathematical kinetic models of phycocyanin release profiles at pH 5.5 and pH 7.4

Hydrogels		Kinetics Models								
		Zero order		First order		Higuchi model		Korsmeyer-Peppas model		
		R^2	K	R^2	K	R^2	K	R^2	K	n
HG-50%	pH **5.5**	0.994	0.017	0.901	0.042	0.965	0.019	0.993	0.039	0.870
	pH **7.4**	0.993	0.013	0.954	0.027	0.976	0.011	0.992	0.030	0.743

3.2. In vitro release studies

HGs have been widely used as a drug delivery system in view of their biocompatibility, biodegradability and swelling properties (Dimatteo et al., 2018). HG architecture facilitates the diffusion of molecules, which makes them interesting for drug release applications (Cui et al., 2022). In the present study, *in vitro* release profiles of Ph from HG-50% in PBS buffers (acidic microenvironment 'pH 5.5' and physiological microenvironment simulation 'pH 7.4') were determined. The cumulative percentage of Ph released, as function of time, are shown in Fig. 5. Indeed, due to its porous nature, HG-50% exhibited a high release dependent on pH conditions, indicating a direct correlation between hydrogel morphology (pore size) and Ph release. As shown in Fig. 5, a faster and sustained Ph release from HG-50% was observed at the acidic microenvironment than the neutral buffer ($p < 0.05$). At pH 7.4, the release rate of selected hydrogel reached about 66.90% after 48 h. This result could be due to the low swelling and degradation degree of the HG-50%, as reported above in swelling and degradation data. Moreover, the slow release at pH 7.4 could be explained by the deprotonation of the amino group of Cs, which makes the internal structure of the hydrogel more compact, hence the difficulty to rapidly release the charged Ph into the hydrogel. However, under acidic conditions, 88.60% of Ph was released after 48 h of incubation from HG-50% (Fig. 5). This may be attributed to the fact that at acidic pH, the amine groups of Cs backbone will be repulsed after protonation, causing a destruction in hydrogel structure, which was in accordance with the *in vitro* degradation outcomes, thus the easily diffusion out of the Ph from the hydrogel (Feki et al., 2020; Risbud et al., 2000). It is interesting to note that the HG-50% could be very promising for controlled drug delivery.

3.3. The kinetics study of phycocyanin release

The widely used kinetic models including zero-order, first-order, Higuchi and Korsmeyer-Peppas models were used to evaluate the *in vitro* release kinetics of the model drug (Ph) from HG-50%, at pH 5.5 and pH 7.4. The regression coefficient (R^2) values and other kinetic constants are summarized in Table 3.

It was revealed that the best equation describing the Ph release from HG-50% was the Korsmeyer-Peppas model. Indeed, the values of correlation coefficient of R^2 obtained from the model were higher than 0.99 ($R^2 > 0.99$). Hence, it should be mentioned that the release data of the HG-50%, tested at pH 5.5 and pH 7.4, was best a good fitted to the control release of Ph.

The diffusion exponent 'n' is indicative of the drug release mechanism: $n = 0.5$ for Fickian diffusion; $0.5 < n < 1.0$ for non-Fickian diffusion/abnormal transport; and $n > 1.0$ for transport of cases II (polymer erosion). As shown in Table 3, the 'n' value was in the range of $0.45 < n < 0.89$ for HG-50% at the two pHs. Therefore, the 'n' value suggested that the release mechanism in our study was non-Fickian diffusion (abnormal diffusion), where diffusion-controlled Ph release refers to the combination of the two

mechanisms of drug release by diffusion followed by matrix erosion controlled by swelling (Ritger and Peppas, 1987; Siepmann and Peppas, 2001). The swelling of the HG was the effective factor in controlling the Ph release. With regard to the rate constant k, its value increases with the pH of the medium. In addition, the k values of Ph release at pH = 5.5 were higher than those at pH = 7.4. This indicates that the release of Ph becomes faster in an acidic medium.

4. Conclusion

The present study aimed to provide an overview of the different properties of chitosan-based hydrogels, as well as composite hydrogels by incorporating BTCP at different ratios (10%, 20% and 50%, w/w). As expected, the addition of BTCP to the chitosan matrix led to better characteristics, including good water retention capacity, better porosity, improved swelling rate and reduced *in vitro* biodegradation at different pHs. Moreover, the increasing of BTCP content in the HG-C increased the tensile strength, resulting in a more elastic and resistant structure. Rheological data show that a higher BTCP content (50%, w/w) increases polymer chain entanglement and reduces chain flexibility. Composite hydrogels also exhibit improved antioxidant properties. Beneficial properties of HG-50% including porosity, swelling ability, stability, biodegradability, and mechanical strength can all be tuned to control the in *vitro release* of the phycocyanin chosen as the model drug.

CRediT authorship contribution statement

Youssra Ben Azaza: Conceptualization, Methodology, Investigation, Validation, Formal analysis, Visualization, Writing – original draft; **Arie van der lee:** Investigation and Methodology; **Suming Li:** Funding acquisition, Supervision; **Moncef Nasri:** Supervision, Editing and Validation; **Rim Nasri:** Resources, Supervision, Funding acquisition, Writing - review & editing.

Declaration of competing interest

The authors declare that they have no known competing financial interests or personal relationships that could have appeared to influence the work reported in this paper.

Data availability

No data was used for the research described in the article.

Acknowledgements

The authors are supported by the Ministry of Higher Education and Scientific Research, Tunisia. We gratefully recognize the financial support from the joint French-Tunisian PHC Utique Program (grant N°: 19G0815).

References

Ahmadi, F., Oveisi, Z., Samani, S.M., Amoozgar, Z., 2015. Chitosan based hydrogels: characteristics and pharmaceutical applications. Res Pharm Sci 10, 1–16.
Ahmed, E.M., 2015. Hydrogel: preparation, characterization, and applications: a review. J. Adv. Res. 6, 105–121. https://doi.org/10.1016/j.jare.2013.07.006.
AOAC Official Method, 2019. AOAC Official Method 924.01Sampling of Liming Materials., 2019. Official Methods of Analysis of AOAC International [Internet]. https://doi.org/10.1093/9780197610138.003.0006. Internet.
Arulmoorthy, M.P., Anbarasi, G., Srinivasan, M., Vishnupriya, B., 2020. Biosynthesis and characterization of chitosan-based hydrogel: a potential in vitro wound healing agent. Mater. Today: Proceedings S2214785320352792. https://doi.org/10.1016/j.matpr.2020.07.186.
Bai, J., Wang, R., Wang, Xiaoming, Liu, S., Wang, Xinliang, Ma, J., Qin, Z., Jiao, T., 2021. Biomineral calcium-ion-mediated conductive hydrogels with high stretchability and self-adhesiveness for sensitive iontronic sensors. Cell Rep. Phys. Sci. 2, 100623. https://doi.org/10.1016/j.xcrp.2021.100623.
Bealer, E.J., Onissema-Karimu, S., Rivera-Galletti, A., Francis, M., Wilkowski, J., Salas-de la Cruz, D., Hu, X., 2020. Protein–polysaccharide composite materials: fabrication and applications. Polymers 12, 464. https://doi.org/10.3390/polym12020464.
Bersuder, P., Hole, M., Smith, G., 1998. Antioxidants from a heated histidine-glucose model system. I: Investigation of the antioxidant role of histidine and isolation of antioxidants by high-performance liquid chromatography. J. Am. Oil Chem. Soc. 75, 181–187. https://doi.org/10.1007/s11746-998-0030-y.
Chai, Q., Jiao, Y., Yu, X., 2017. Hydrogels for biomedical applications: their characteristics and the mechanisms behind them. Gels 3, 6. https://doi.org/10.3390/gels3010006.
Chang, C., Lue, A., Zhang, L., 2008. Effects of crosslinking methods on structure and properties of cellulose/PVA hydrogels. Macromol. Chem. Phys. 209, 1266–1273. https://doi.org/10.1002/macp.200800161.
Chen, M., Ren, X., Dong, L., Li, X., Cheng, H., 2021. Preparation of dynamic covalently crosslinking keratin hydrogels based on thiol/disulfide bonds exchange strategy. Int. J. Biol. Macromol. 182, 1259–1267. https://doi.org/10.1016/j.ijbiomac.2021.05.057.
Chen, X., Fan, M., Tan, H., Ren, B., Yuan, G., Jia, Y., Li, J., Xiong, D., Xing, X., Niu, X., Hu, X., 2019. Magnetic and self-healing chitosan-alginate hydrogel encapsulated gelatin microspheres via covalent cross-linking for drug delivery. Mater. Sci. Eng. C 101, 619–629. https://doi.org/10.1016/j.msec.2019.04.012.
Cruz, M.V., Jacobowski, A.C., Macedo, M.L.R., Batista, K.A., Fernandes, K.F., 2019. Immobilization of antimicrobial trypsin inhibitors onto cashew gum polysaccharide/PVA films. Int. J. Biol. Macromol. 127, 433–439. https://doi.org/10.1016/j.ijbiomac.2019.01.010.
Cui, T., Wu, Y., Ni, C., Sun, Y., Cheng, J., 2022. Rheology and texture analysis of gelatin/dialdehyde starch hydrogel carriers for curcumin controlled release. Carbohydr. Polym. 283, 119154. https://doi.org/10.1016/j.carbpol.2022.119154.
Darge, H.F., Andrgie, A.T., Tsai, H.-C., Lai, J.-Y., 2019. Polysaccharide and polypeptide based injectable thermo-sensitive hydrogels for local biomedical applications. Int. J. Biol. Macromol. 133, 545–563. https://doi.org/10.1016/j.ijbiomac.2019.04.131.
Decker, E.A., Welch, B., 1990. Role of ferritin as a lipid oxidation catalyst in muscle food. J. Agric. Food Chem. 38, 674–677. https://doi.org/10.1021/jf00093a019.
Dimatteo, R., Darling, N.J., Segura, T., 2018. In situ forming injectable hydrogels for drug delivery and wound repair. Adv. Drug Deliv. Rev. 127, 167–184. https://doi.org/10.1016/j.addr.2018.03.007.
Duan, J., Liang, X., Cao, Y., Wang, S., Zhang, L., 2015. High strength chitosan hydrogels with biocompatibility via new avenue based on constructing nanofibrous architecture. Macromolecules 48, 2706–2714. https://doi.org/10.1021/acs.macromol.5b00117.
Duceac, I.A., Vereştiuc, L., Coroaba, A., Arotăriţei, D., Coseri, S., 2021. All-polysaccharide hydrogels for drug delivery applications: tunable chitosan beads surfaces via physical or chemical interactions, using oxidized pullulan. Int. J. Biol. Macromol. 181, 1047–1062. https://doi.org/10.1016/j.ijbiomac.2021.04.128.
Feki, A., Hamdi, M., Jaballi, I., Zghal, S., Nasri, M., Ben Amara, I., 2020. Conception and characterization of a multi-sensitive composite chitosan-red marine alga-

polysaccharide hydrogels for insulin controlled-release. Carbohydr. Polym. 236, 116046. https://doi.org/10.1016/j.carbpol.2020.116046.
Feng, E., Ma, G., Wu, Y., Wang, H., Lei, Z., 2014. Preparation and properties of organic–inorganic composite superabsorbent based on xanthan gum and loess. Carbohydr. Polym. 111, 463–468. https://doi.org/10.1016/j.carbpol.2014.04.031.
Figueroa-Pizano, M.D., Vélaz, I., Peñas, F.J., Zavala-Rivera, P., Rosas-Durazo, A.J., Maldonado-Arce, A.D., Martínez-Barbosa, M.E., 2018. Effect of freeze-thawing conditions for preparation of chitosan-poly (vinyl alcohol) hydrogels and drug release studies. Carbohydr. Polym. 195, 476–485. https://doi.org/10.1016/j.carbpol.2018.05.004.
Gull, N., Khan, S.M., Khalid, S., Zia, S., Islam, A., Sabir, A., Sultan, M., Hussain, F., Khan, R.U., Butt, M.T.Z., 2020. Designing of biocompatible and biodegradable chitosan based crosslinked hydrogel for in vitro release of encapsulated povidone-iodine: a clinical translation. Int. J. Biol. Macromol. 164, 4370–4380. https://doi.org/10.1016/j.ijbiomac.2020.09.031.
Guo, B., Qu, J., Zhao, X., Zhang, M., 2019. Degradable conductive self-healing hydrogels based on dextran-graft-tetraaniline and N-carboxyethyl chitosan as injectable carriers for myoblast cell therapy and muscle regeneration. Acta Biomater. 84, 180–193. https://doi.org/10.1016/j.actbio.2018.12.008.
Hamdi, M., Feki, A., Bardaa, S., Li, S., Nagarajan, S., Mellouli, M., Boudawara, T., Sahnoun, Z., Nasri, M., Nasri, R., 2020. A novel blue crab chitosan/protein composite hydrogel enriched with carotenoids endowed with distinguished wound healing capability: in vitro characterization and in vivo assessment. Mater. Sci. Eng. C 113, 110978. https://doi.org/10.1016/j.msec.2020.110978.
Hamdi, M., Hajji, S., Affes, S., Taktak, W., Maâlej, H., Nasri, M., Nasri, R., 2018. Development of a controlled bioconversion process for the recovery of chitosan from blue crab (Portunus segnis) exoskeleton. Food Hydrocolloids 77, 534–548. https://doi.org/10.1016/j.foodhyd.2017.10.031.
Hamdi, M., Nasri, R., Hajji, S., Nigen, M., Li, S., Nasri, M., 2019. Acetylation degree, a key parameter modulating chitosan rheological, thermal and film-forming properties. Food Hydrocolloids 87, 48–60. https://doi.org/10.1016/j.foodhyd.2018.07.027.
Hosseini, S.F., Rezaei, M., Zandi, M., Farahmandghavi, F., 2015. Fabrication of bio-nanocomposite films based on fish gelatin reinforced with chitosan nanoparticles. Food Hydrocolloids 44, 172–182. https://doi.org/10.1016/j.foodhyd.2014.09.004.
Islam, A., Yasin, T., 2012. Controlled delivery of drug from pH sensitive chitosan/poly (vinyl alcohol) blend. Carbohydr. Polym. 88, 1055–1060. https://doi.org/10.1016/j.carbpol.2012.01.070.
Jafari, A., Hassanajili, S., Azarpira, N., Bagher Karimi, M., Geramizadeh, B., 2019. Development of thermal-crosslinkable chitosan/maleic terminated polyethylene glycol hydrogels for full thickness wound healing: in vitro and in vivo evaluation. Eur. Polym. J. 118, 113–127. https://doi.org/10.1016/j.eurpolymj.2019.05.046.
Lima, D.S., Tenório-Neto, E.T., Lima-Tenório, M.K., Guilherme, M.R., Scariot, D.B., Nakamura, C.V., Muniz, E.C., Rubira, A.F., 2018. pH-responsive alginate-based hydrogels for protein delivery. J. Mol. Liq. 262, 29–36. https://doi.org/10.1016/j.molliq.2018.04.002.
Liu, X., Yang, W., Xiao, C., 2019. Self-healable and pH-sensitive high-strength water-soluble chitosan/chemically cross-linked polyvinyl alcohol semi-IPN hydrogel. Int. J. Biol. Macromol. 138, 667–672. https://doi.org/10.1016/j.ijbiomac.2019.07.169.
Magli, S., Rossi, G.B., Risi, G., Bertini, S., Cosentino, C., Crippa, L., Ballarini, E., Cavaletti, G., Piazza, L., Masseroni, E., Nicotra, F., Russo, L., 2020. Design and synthesis of chitosan—Gelatin hybrid hydrogels for 3D printable in vitro models. Front. Chem. 8.
Marapureddy, S.G., Thareja, P., 2020. Structure and rheology of hydrogels: applications in drug delivery. In: Chandra, P., Pandey, L.M. (Eds.), Biointerface Engineering: Prospects in Medical Diagnostics and Drug Delivery. Springer Singapore, Singapore, pp. 75–99. https://doi.org/10.1007/978-981-15-4790-4_4.
Mohebi, E., Shahbazi, Y., 2016. Application of chitosan and gelatin based active packaging films for peeled shrimp preservation: a novel functional wrapping design. LWT - Food Sci. Technol. 76. https://doi.org/10.1016/j.lwt.2016.10.062.
Nie, J., Wang, Z., Hu, Q., 2016. Difference between chitosan hydrogels via alkaline and acidic solvent systems. Sci. Rep. 6, 36053. https://doi.org/10.1038/srep36053.
Phan, V.H.G., Mathiyalagan, R., Nguyen, M.-T., Tran, T.-T., Murugesan, M., Ho, T.-N., Huong, H., Yang, D.C., Li, Y., Thambi, T., 2022. Ionically cross-linked alginate-chitosan core-shell hydrogel beads for oral delivery of insulin. Int. J. Biol. Macromol. 222, 262–271. https://doi.org/10.1016/j.ijbiomac.2022.09.165.
Pita-López, M.L., Fletes-Vargas, G., Espinosa-Andrews, H., Rodríguez-Rodríguez, R., 2021. Physically cross-linked chitosan-based hydrogels for tissue engineering applications: a state-of-the-art review. Eur. Polym. J. 145, 110176. https://doi.org/10.1016/j.eurpolymj.2020.110176.
Raj Singh, T.R., McCarron, P.A., Woolfson, A.D., Donnelly, R.F., 2009. Investigation of swelling and network parameters of poly(ethylene glycol)-crosslinked poly (methyl vinyl ether-co-maleic acid) hydrogels. Eur. Polym. J. 45, 1239–1249. https://doi.org/10.1016/j.eurpolymj.2008.12.019.
Rasool, A., Ata, S., Islam, A., 2019a. Stimuli responsive biopolymer (chitosan) based blend hydrogels for wound healing application. Carbohydr. Polym. 203, 423–429. https://doi.org/10.1016/j.carbpol.2018.09.083.
Rawdkuen, S., Sai-Ut, S., Khamsorn, S., Chaijan, M., Benjakul, S., 2009. Biochemical and gelling properties of tilapia surimi and protein recovered using an acid-alkaline process. Food Chem. 112, 112–119. https://doi.org/10.1016/j.foodchem.2008.05.047.
Risbud, M.V., Hardikar, A.A., Bhat, S.V., Bhonde, R.R., 2000. pH-sensitive freeze-dried chitosan–polyvinyl pyrrolidone hydrogels as controlled release system for antibiotic delivery. J. Contr. Release 68, 23–30. https://doi.org/10.1016/S0168-3659(00)00208-X.
Ritger, P.L., Peppas, N.A., 1987. A simple equation for description of solute release II. Fickian and anomalous release from swellable devices. J. Contr. Release 5, 37–42. https://doi.org/10.1016/0168-3659(87)90035-6.
Shi, Z., Gao, X., Ullah, M.W., Li, S., Wang, Q., Yang, G., 2016. Electroconductive natural polymer-based hydrogels. Biomaterials 111, 40–54. https://doi.org/10.1016/j.biomaterials.2016.09.020.
Siepmann, J., Peppas, N.A., 2001. Modeling of drug release from delivery systems based on hydroxypropyl methylcellulose (HPMC). Advanced Drug Delivery Reviews. Math. Model. Controlled Drug Deliv. 48, 139–157. https://doi.org/10.1016/S0169-409X(01)00112-0.
Song, J., Yuan, C., Jiao, T., Xing, R., Yang, M., Adams, D.J., Yan, X., 2020. Multifunctional antimicrobial biometallohydrogels based on amino acid coordinated self-assembly. Small 16, 1907309. https://doi.org/10.1002/smll.201907309.
Tuan Mohamood, N.F.A.-Z., Zainuddin, N., Ahmad@Ayob, M., Tan, S.W., 2018. Preparation, optimization and swelling study of carboxymethyl sago starch (CMSS) –acid hydrogel. Chem. Cent. J. 12, 133. https://doi.org/10.1186/s13065-018-0500-8.
Voron'ko, N.G., Derkach, S.R., Kuchina, Y.A., Sokolan, N.I., 2016. The chitosan–gelatin (bio)polyelectrolyte complexes formation in an acidic medium. Carbohydr. Polym. 138, 265–272. https://doi.org/10.1016/j.carbpol.2015.11.059.
Wang, Xiaoming, Wang, Xinliang, Yin, J., Li, N., Zhang, Z., Xu, Y., Zhang, L., Qin, Z., Jiao, T., 2022. Mechanically robust, degradable and conductive MXene-composited gelatin organohydrogel with environmental stability and self-adhesiveness for multifunctional sensor. Compos. B Eng. 241, 110052. https://doi.org/10.1016/j.compositesb.2022.110052.
Wei, J., Wei, G., Shang, Y., Zhou, J., Wu, C., Wang, Q., 2019. Dissolution–crystallization transition within a polymer hydrogel for a processable ultratough electrolyte. Adv. Mater. 1900248. https://doi.org/10.1002/adma.201900248.
Wei, W., Li, J., Qi, X., Zhong, Y., Zuo, G., Pan, X., Su, T., Zhang, J., Dong, W., 2017. Synthesis and characterization of a multi-sensitive polysaccharide hydrogel for drug delivery. Carbohydr. Polym. 177, 275–283. https://doi.org/10.1016/j.carbpol.2017.08.133.
Wu, D., Xu, J., Chen, Y., Yi, M., Wang, Q., 2018. Gum Arabic: a promising candidate for the construction of physical hydrogels exhibiting highly stretchable, self-healing and tensility reinforcing performances. Carbohydr. Polym. 181, 167–174. https://doi.org/10.1016/j.carbpol.2017.10.076.
Xing, L., Sun, J., Tan, H., Yuan, G., Li, J., Jia, Y., Xiong, D., Chen, G., Lai, J., Ling, Z., Chen, Y., Niu, X., 2019. Covalently polysaccharide-based alginate/chitosan hydrogel embedded alginate microspheres for BSA encapsulation and soft tissue engineering. Int. J. Biol. Macromol. 127, 340–348. https://doi.org/10.1016/j.ijbiomac.2019.01.065.
Xing, R., Liu, K., Jiao, T., Zhang, N., Ma, K., Zhang, R., Zou, Q., Ma, G., Yan, X., 2016. An injectable self-assembling collagen–gold hybrid hydrogel for combinatorial antitumor photothermal/photodynamic therapy. Adv. Mater. 28, 3669–3676. https://doi.org/10.1002/adma.201600284.
Yan, J., Wang, Yu, Zhang, X., Zhao, X., Ma, J., Pu, X., Wang, Yonggang, Ran, F., Wang, Yanling, Leng, F., Zhang, W., 2019. Snakegourd root/Astragalus polysaccharide hydrogel preparation and application in 3D printing. Int. J. Biol. Macromol. 121, 309–316. https://doi.org/10.1016/j.ijbiomac.2018.10.008.
Yildirim, A., Mavi, A., Kara, A.A., 2001. Determination of antioxidant and antimicrobial activities of Rumex crispus L. extracts. J. Agric. Food Chem. 49, 4083–4089. https://doi.org/10.1021/jf0103572.
Zhou, Z., Zhang, X., Xu, L., Lu, H., Chen, Y., Wu, C., Hu, P., 2022. A self-healing hydrogel based on crosslinked hyaluronic acid and chitosan to facilitate diabetic wound healing. Int. J. Biol. Macromol. 220, 326–336. https://doi.org/10.1016/j.ijbiomac.2022.08.076.